Photon PDF and heavy flavors in the CT18 global analysis

Keping Xie[1] and Marco Guzzi[2]

[1]PITT PACC, University of Pittsburgh

[2]Kennesaw State University

EPS-HEP 2021, 26 July 2021

Photon PDF with Tim J. Hobbs (IIT), Tie-Jiun Hou (Northeastern U., China), Carl Schmidt (MSU), Mengshi Yan (PKU), and C.-P. Yuan (MSU), 2106.10299
Heavy Flavors with Pavel Nadolsky (SMU), ongoing

Outline

The precision requirements

The precision requirements

- The LHC becomes a precision machine.
- Theoretical cross sections have been achieved at NNLO in QCD, $\mathscr{O}(\alpha_s^2)$, for many processes.
- Due to $\alpha_e \sim \alpha_s^2$, we expect the QED corrections are the same level.
- The photon-initiated processes $(\gamma + \gamma, q, g \to X)$ will have observable effects.

Many applications

The SM processes

- Drell-Yan: $\ell^+\ell^-$
- $W^\pm H$
- W^+W^-

BSM scenarios

- Heavy leptons: L^+L^-
- Charged Higgs: $H^\pm, H^{\pm\pm}$

The existing photon PDFs

The first generation

- MRST2004QED [0411040] models the photon PDF with an effective mass scale.
- NNPDF23QED [1308.0598] and NNPDF3.0QED [1410.8849] constrains photon PDF with the LHC Drell-Yan data, $q\bar{q}, \gamma\gamma \to \ell^+\ell^-$
- CT14qed_inc fits the inelastic ZEUS $ep \to e\gamma + X$ data [1509.02905], and include elastic component as well.

The second generation

- Recently, LUXqed directly takes the structure functions $F_{2,L}(x, Q^2)$ to constrain photon PDF uncertainty down to percent level [1607.04266,1708.01256]
- NNPDF3.1luxqed [1712.07053] initializes photon PDF with LUX formula at $Q = 100\ \mathrm{GeV}$ (a high scale) and evolves DGLAP equation both upwardly and downwardly.
- MMHT2015qed [1907.02750] initializes photon at 1 GeV (a low scale) and evolve DGLAP upwardly.
- Our work incorporates the LUX formalism with the CT18 [1912.10053] global analysis.

Two approaches: LUX vs DGLAP

- CT18lux: directly calculate the photon PDF with the LUX formalism
- CT18qed: initialize the inelastic photon PDF with the LUX formalism at low scales, and evolve the $\mathrm{QED}_{\mathrm{NLO}} \otimes \mathrm{QCD}_{\mathrm{NNLO}}$ DGLAP equations up to high scales, similar to MMHT2015qed.

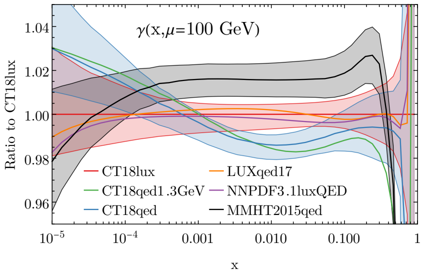

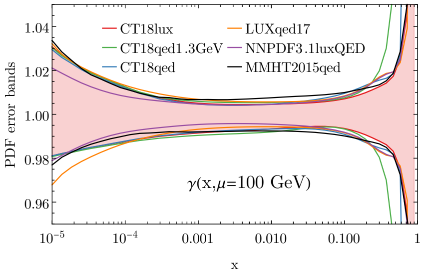

The take-home message:

- In the intermediate-x region, all photon PDFs give similar error bands.
- CT18lux photon PDF is in between LUXqed (also, NNPDF3.1luxQED) and MMHT2015qed, while CT18qed gives a smaller photon PDF.
- In the large-x region, the DGLAP approach (for both MMHT2015qed and CT18qed) gives a smaller photon than the LUX approach.

Photon PDF uncertainties

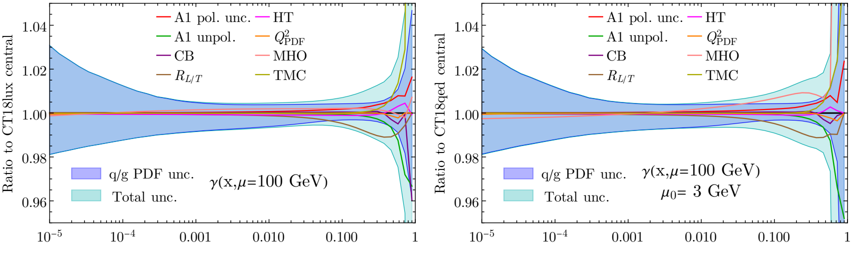

- A1 pol. unc.: the uncertainty of the A1 fit of the world polarized data
- A1 unpol.: Switching to A1 fit of the world unpolarized data
- CB: Changing resonance SF from CLAS to Christy-Bosted fit
- Variations of $R_{L/T} = \sigma_L/\sigma_T$ by 50% [1708.01256]
- HT: Adding higher-twist contribution to F_L [1708.01256] and F_2 [1602.03154].
- $Q^2_{\rm PDF}$: changing the matching scale $9 \to 5 \;\; \mathrm{GeV}^2$
- MHO: varying the scale to estimate the missing high-order uncertainty
- TMC: adding the target mass correction to the SFs.

The applications

W^+H production

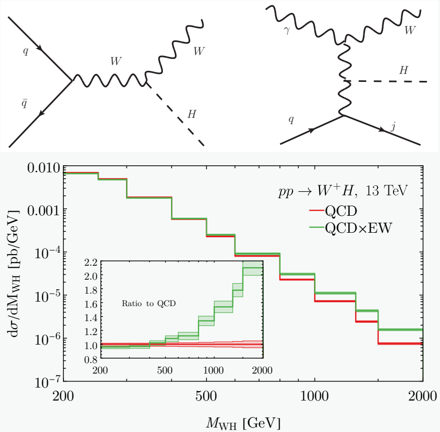

Exclusive $\gamma\gamma \to W^+W^-$

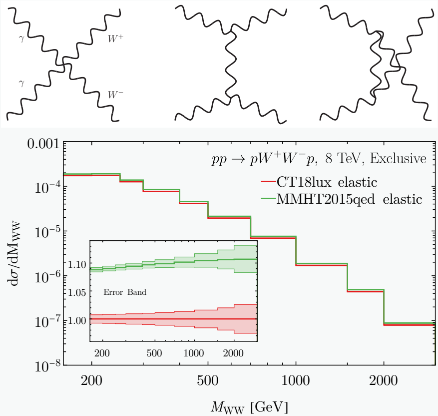

- At a large invariant mass, the photon initiated processes make a significant contribution
- CT18lux elastic photon (including both quarks and leptons) is smaller than MMHT2015qed one (only including quarks).

Summary and conclusions

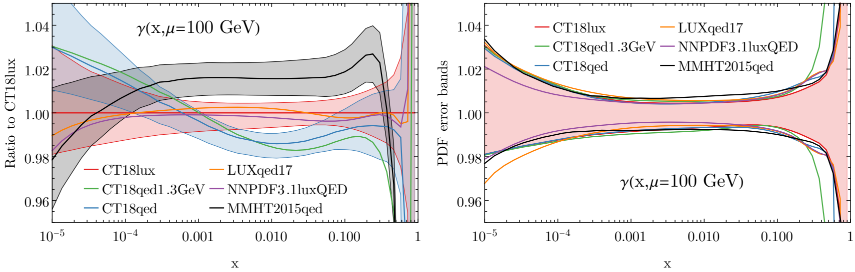

- We have two photon PDF sets, CT18lux and CT18qed, based on the LUX and DGLAP approach, respectively.
- The overall uncertainties agree with the LUXqed(also NNPDF3.1luxQED) and MMHT2015qed.
- In the intermediate-x region, CT18lux is in between the LUXqed(also NNPDF3.1luxQED) and MMHT2015qed, while CT18qed is smaller.
- In the small-x region, the CT18qed is lager than CT18lux, due to the equivalent LO SF. The MMHT2015qed becomes smaller because of the smaller singlet PDFs Σ_e.
- In the large-x region, the DGLAP approach (MMHT2015qed and CT18qed) give smaller PDFs due to the non-perturbative SFs.
- The low-μ_0 DGLAP approach gives larger uncertainty at large x, due to non-perturbative SFs at low scales.

Outline

The CT18 analysis

PHYSICAL REVIEW D **103,** 014013 (2021)

Editors' Suggestion

New CTEQ global analysis of quantum chromodynamics with high-precision data from the LHC

Tie-Jiun Hou,[1,†] Jun Gao,[2] T. J. Hobbs,[3,4] Keping Xie,[3,5] Sayipjamal Dulat,[6,‡] Marco Guzzi,[7] Joey Huston,[8] Pavel Nadolsky,[3,§] Jon Pumplin,[8,*] Carl Schmidt,[8] Ibrahim Sitiwaldi,[6] Daniel Stump,[8] and C.-P. Yuan[8,∥]

TABLE I. Datasets included in the CT18(Z) NNLO global analyses. Here we directly compare the quality of fit found for CT18 NNLO vs CT18Z NNLO on the basis of χ^2_E, $\chi^2_E/N_{pt,E}$, and S_E, in which $N_{pt,E}$, χ^2_E are the number of points and value of χ^2 for experiment E at the global minimum. S_E is the effective Gaussian parameter [38,42,56] quantifying agreement with each experiment. The ATLAS 7 TeV 35 pb^{-1} W/Z dataset, marked by ‡‡, is replaced by the updated one (4.6 fb^{-1}) in the CT18A and CT18Z fits. The CDHSW data, labeled by †, are not included in the CT18Z fit. The numbers in parentheses are for the CT18Z NNLO fit.

Exp. ID#	Experimental dataset		$N_{pt,E}$	χ^2_E	$\chi^2_E/N_{pt,E}$	S_E
160	HERAI + II 1 fb^{-1}, H1 and ZEUS NC and CC $e^{\pm}p$ reduced cross sec. comb.	[30]	1120	1408 (1378)	1.3 (1.2)	5.7 (5.1)
101	BCDMS F_2^p	[57]	337	374 (384)	1.1 (1.1)	1.4 (1.8)
102	BCDMS F_2^d	[58]	250	280 (287)	1.1 (1.1)	1.3 (1.6)
104	NMC F_2^d/F_2^p	[59]	123	126 (116)	1.0 (0.9)	0.2 (−0.4)
108†	CDHSW F_2^p	[60]	85	85.6 (86.8)	1.0 (1.0)	0.1 (0.2)
109†	CDHSW $x_B F_3^p$	[60]	96	86.5 (85.6)	0.9 (0.9)	−0.7 (−0.7)
110	CCFR F_2^p	[61]	69	78.8 (76.0)	1.1 (1.1)	0.9 (0.6)
111	CCFR $x_B F_3^p$	[62]	86	33.8 (31.4)	0.4 (0.4)	−5.2 (−5.6)
124	NuTeV $\nu\mu\mu$ SIDIS	[63]	38	18.5 (30.3)	0.5 (0.8)	−2.7 (−0.9)
125	NuTeV $\bar{\nu}\mu\mu$ SIDIS	[63]	33	38.5 (56.7)	1.2 (1.7)	0.7 (2.5)
126	CCFR $\nu\mu\mu$ SIDIS	[64]	40	29.9 (35.0)	0.7 (0.9)	−1.1 (−0.5)
127	CCFR $\bar{\nu}\mu\mu$ SIDIS	[64]	38	19.8 (18.7)	0.5 (0.5)	−2.5 (−2.7)
145	H1 σ_r^b	[65]	10	6.8 (7.0)	0.7 (0.7)	−0.6 (−0.6)
147	Combined HERA charm production	[66]	47	58.3 (56.4)	1.2 (1.2)	1.1 (1.0)
169	H1 F_L	[33]	9	17.0 (15.4)	1.9 (1.7)	1.7 (1.4)
201	E605 Drell-Yan process	[67]	119	103.4 (102.4)	0.9 (0.9)	−1.0 (−1.1)
203	E866 Drell-Yan process $\sigma_{pd}/(2\sigma_{pp})$	[68]	15	16.1 (17.9)	1.1 (1.2)	0.3 (0.6)
204	E866 Drell-Yan process $Q^3 d^2\sigma_{pp}/(dQ dx_F)$	[69]	184	244 (240)	1.3 (1.3)	2.9 (2.7)
225	CDF run-1 lepton A_{ch}, $p_{T\ell} > 25$ GeV	[70]	11	9.0 (9.3)	0.8 (0.8)	−0.3 (−0.2)
227	CDF run-2 electron A_{ch}, $p_{T\ell} > 25$ GeV	[71]	11	13.5 (13.4)	1.2 (1.2)	0.6 (0.6)
234	DØ run-2 muon A_{ch}, $p_{T\ell} > 20$ GeV	[72]	9	9.1 (9.0)	1.0 (1.0)	0.2 (0.1)
260	DØ run-2 Z rapidity	[73]	28	16.9 (18.7)	0.6 (0.7)	−1.7 (−1.3)
261	CDF run-2 Z rapidity	[74]	29	48.7 (61.1)	1.7 (2.1)	2.2 (3.3)
266	CMS 7 TeV 4.7 fb^{-1}, muon A_{ch}, $p_{T\ell} > 35$ GeV	[75]	11	7.9 (12.2)	0.7 (1.1)	−0.6 (0.4)
267	CMS 7 TeV 840 pb^{-1}, electron A_{ch}, $p_{T\ell} > 35$ GeV	[76]	11	4.6 (5.5)	0.4 (0.5)	−1.6 (−1.3)
268‡‡	ATLAS 7 TeV 35 pb^{-1} W/Z cross sec., A_{ch}	[77]	41	44.4 (50.6)	1.1 (1.2)	0.4 (1.1)
281	DØ run-2 9.7 fb^{-1} electron A_{ch}, $p_{T\ell} > 25$ GeV	[78]	13	22.8 (20.5)	1.8 (1.6)	1.7 (1.4)
504	CDF run-2 inclusive jet production	[79]	72	122 (117)	1.7 (1.6)	3.5 (3.2)
514	DØ run-2 inclusive jet production	[80]	110	113.8 (115.2)	1.0 (1.0)	0.3 (0.4)

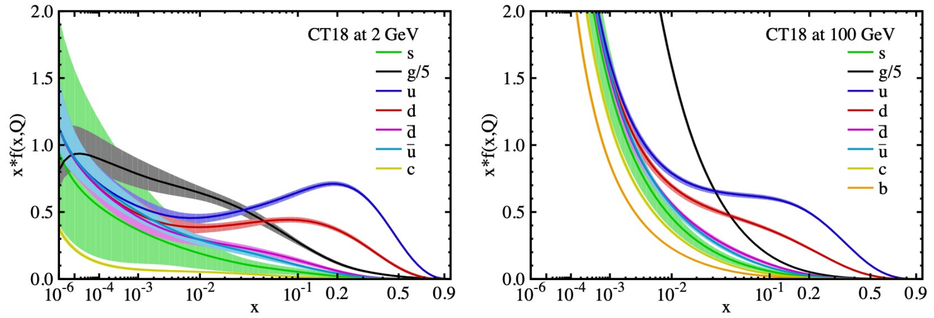

TABLE II. Like Table I, for newly included LHC measurements. The ATLAS 7 TeV W/Z data (4.6 fb^{-1}), labeled by ‡, are included in the CT18A and CT18Z global fits, but not in CT18 and CT18X.

Exp. ID#	Experimental dataset		$N_{pt,E}$	χ^2_E	$\chi^2_E/N_{pt,E}$	S_E
245	LHCb 7 TeV 1.0 fb^{-1} W/Z forward rapidity cross sec.	[81]	33	53.8 (39.9)	1.6 (1.2)	2.2 (0.9)
246	LHCb 8 TeV 2.0 fb^{-1} $Z \to e^- e^+$ forward rapidity cross sec.	[82]	17	17.7 (18.0)	1.0 (1.1)	0.2 (0.3)
248‡	ATLAS 7 TeV 4.6 fb^{-1}, W/Z combined cross sec.	[39]	34	287.3 (88.7)	8.4 (2.6)	13.7 (4.8)
249	CMS 8 TeV 18.8 fb^{-1} muon charge asymmetry A_{ch}	[83]	11	11.4 (12.1)	1.0 (1.1)	0.2 (0.4)
250	LHCb 8 TeV 2.0 fb^{-1} W/Z cross sec.	[84]	34	73.7 (59.4)	2.1 (1.7)	3.7 (2.6)
253	ATLAS 8 TeV 20.3 fb^{-1}, Z p_T cross sec.	[85]	27	30.2 (28.3)	1.1 (1.0)	0.5 (0.3)
542	CMS 7 TeV 5 fb^{-1}, single incl. jet cross sec., $R = 0.7$ (extended in y)	[86]	158	194.7 (188.6)	1.2 (1.2)	2.0 (1.7)
544	ATLAS 7 TeV 4.5 fb^{-1}, single incl. jet cross sec., $R = 0.6$	[9]	140	202.7 (203.0)	1.4 (1.5)	3.3 (3.4)
545	CMS 8 TeV 19.7 fb^{-1}, single incl. jet cross sec., $R = 0.7$, (extended in y)	[87]	185	210.3 (207.6)	1.1 (1.1)	1.3 (1.2)
573	CMS 8 TeV 19.7 fb^{-1}, $t\bar{t}$ norm. double-diff. top p_T and y cross sec.	[88]	16	18.9 (19.1)	1.2 (1.2)	0.6 (0.6)
580	ATLAS 8 TeV 20.3 fb^{-1}, $t\bar{t}$ p_T^t and $m_{t\bar{t}}$ abs. spectrum	[89]	15	9.4 (10.7)	0.6 (0.7)	−1.1 (−0.8)

Heavy-flavor production measurements at HERA and LHC currently included in CT18.

Impact of c/b production measurements in semi-inclusive DIS on PDFs in the CT18 global QCD analysis

c/b procution kinematics in CT18

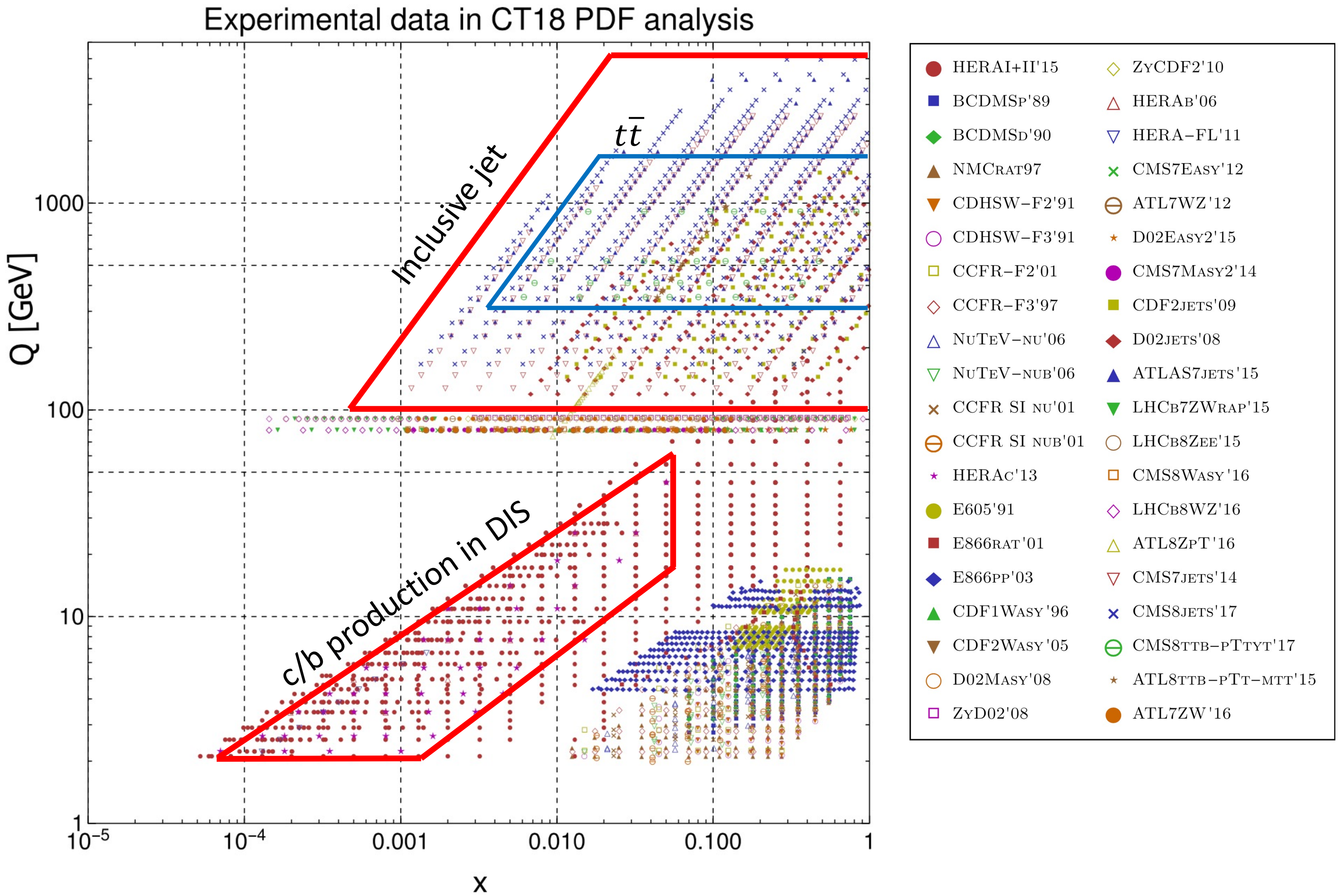

Impact on the gluon PDF at intermediate and small x.

Indirect constraints on strangeness.

2018: New Combination of charm and beauty production at HERA, EPJC (2018), [arXiv:1804.01019].
This analysis extends previous H1 and ZEUS combination of *c* measurements in DIS (EPJC73, (2013) [arXiv:1211.1182]), and includes new *c* and *b* data.

Dataset	PDF (scheme)	χ^2 [p-value]
charm [38]	HERAPDF20_NLO_FF3A (FFNS)	59 [0.23]
	ABKM09 (FFNS)	59 [0.23]
	ABMP16_3_nlo (FFNS)	61 [0.18]
	ABMP16_3_nnlo (FFNS)	70 [0.05]
	HERAPDF20_NLO_EIG (RTOPT)	71 [0.04]
(N_{data} = 52)	HERAPDF20_NNLO_EIG (RTOPT)	66 [0.09]
	NNPDF31sx NNLO (FONLL-C)	106 [$1.5 \cdot 10^{-6}$]
(N_{data} = 47)	NNPDF31sx NNLO+NLLX (FONLL-C)	71 [0.013]
charm, this analysis	HERAPDF20_NLO_FF3A (FFNS)	86 [0.002]
	ABKM09 (FFNS)	82 [0.005]
	ABMP16_3_nlo (FFNS)	90 [0.0008]
	ABMP16_3_nnlo (FFNS)	109 [$6 \cdot 10^{-6}$]
	HERAPDF20_NLO_EIG (RTOPT)	99 [$9 \cdot 10^{-5}$]
(N_{data} = 52)	HERAPDF20_NNLO_EIG (RTOPT)	102 [$4 \cdot 10^{-5}$]
	NNPDF31sx NNLO (FONLL-C)	140 [$1.5 \cdot 10^{-11}$]
(N_{data} = 47)	NNPDF31sx NNLO+NLLX (FONLL-C)	114 [$5 \cdot 10^{-7}$]
beauty, this analysis	HERAPDF20_NLO_FF3A (FFNS)	33[0.20]
	ABMP16_3_nlo (FFNS)	37 [0.10]
	ABMP16_3_nnlo (FFNS)	41 [0.04]
	HERAPDF20_NLO_EIG (RTOPT)	33 [0.20]
(N_{data} = 27)	HERAPDF20_NNLO_EIG (RTOPT)	45 [0.016]

Table 4: The χ^2, p-values and number of data points of the charm and beauty data with respect to the NLO and approximate NNLO calculations using various PDFs as described in the text. The measurements at $Q^2 = 2.5$ GeV^2 are excluded in the calculations of the χ^2 values for the NNPDF3.1sx predictions, by which the number of data points is reduced to 47, as detailed in the caption of figure 12.

CT18NNLO with new *c* and *b* combination

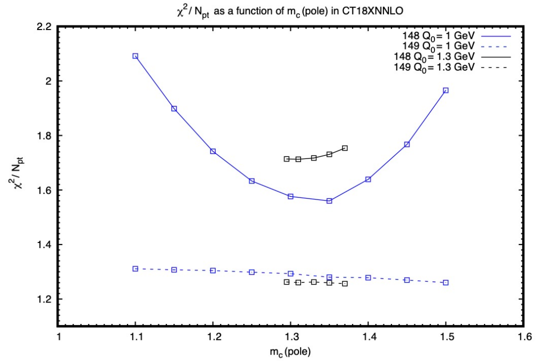

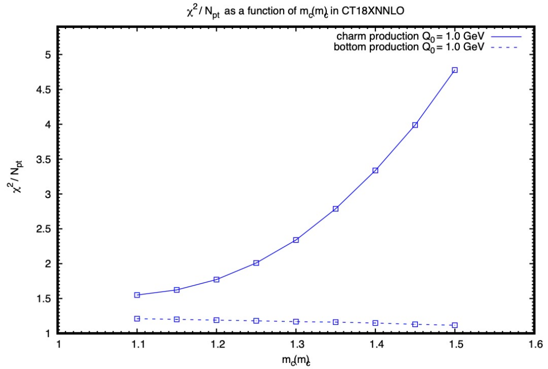

CT18 global fit discussed in this talk

NNPDF4.0: Fit quality – NNLO

Data set	$N_{\rm dat}$	$\chi^2/N_{\rm dat}$
Fixed-target DIS	1881	1.10
HERA	1208	1.21
σ_c	37	2.11
σ_b	26	1.48
Fixed-target Drell-Yan	189	1.00
CDF	28	1.31
D0	37	1.00

Overall good description of the data sets

Two exceptions:
HERA σ_c and ATLAS top pair

Weighted fits analysis:
in case of HERA σ_c:
lack of small-x resummation

See E. Nocera's Talk PDF4LHC March 22nd 2021

MSHT2020 global PDF analysis 2012.04684 [hep-ph]

We remove the combined HERA data on $F_c(x, Q^2)$ [89] and use the final combined data on both $F_c(x, Q^2)$ and $F_b(x, Q^2)$ including full information on the statistical and systematic correlations between them [26]. The fit quality, with $\chi^2/N_{\rm pts} = 1.68$ for 79 points at NNLO, is rather higher than one might expect. However, this appears to be similar to predictions from other groups

See R. Thorne's talk PDF4LHC March 22nd 2021

Combined charm and bottom HERA SIDIS data
(H1 and ZEUS Coll. 1804.01019) in the CT18 analysis

WORK IN PROGRESS

We explored the following alternative settings in various combinations:

- Fits with increased weights of HERA HQ SIDIS data
- alternative parametrizations of the gluon
- varied MS-bar and pole m_c
- varied initial scale Q_0
- varied parameters of the x-dependent DIS factorization scale
- varied S-ACOT-χ rescaling parameter

For large weights of the HERA c/b data, the opposing χ^2 pulls arise from:
LHCb 7 and 8 TeV W/Z Xsec, ATLAS 7 and CDF Run-2 incl. jets, CDF Run-2 Z rapidity and D0 Run-2 ele A_{ch} data.

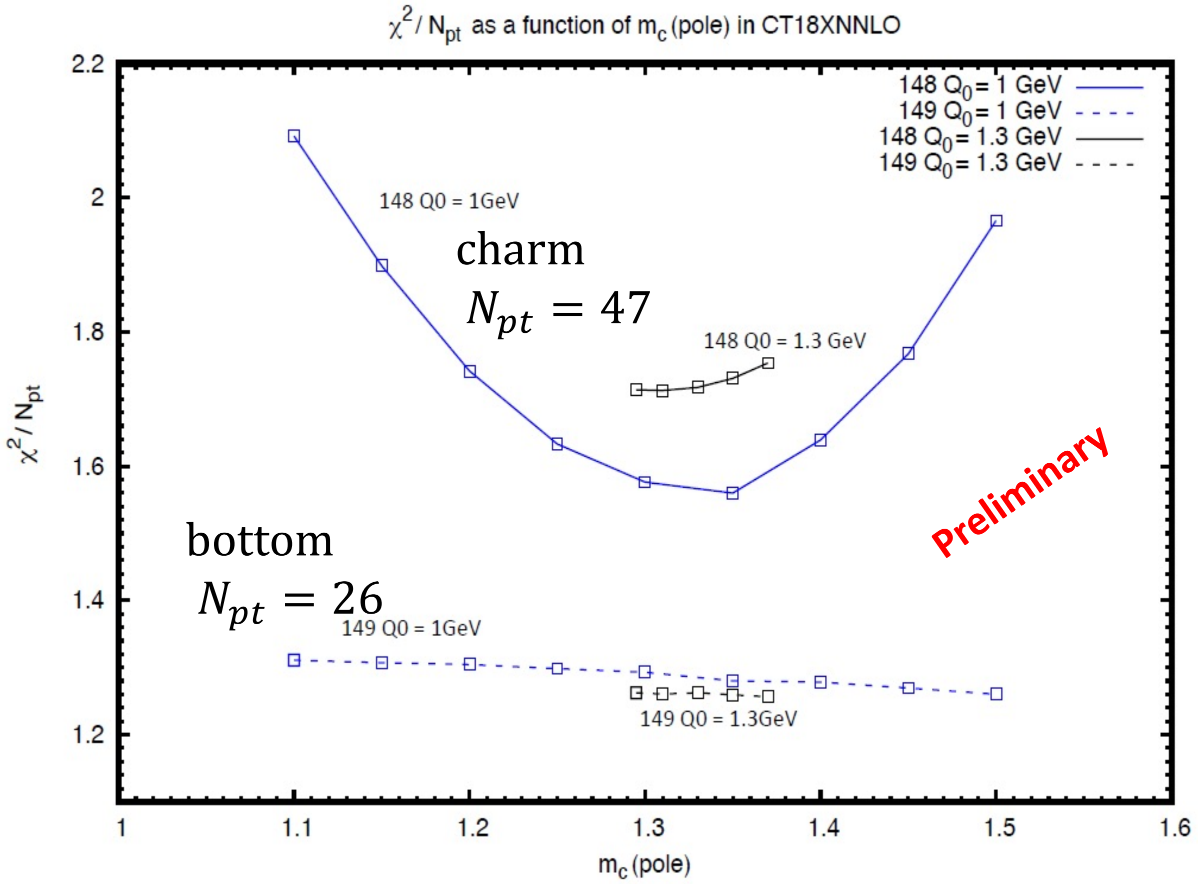

CT18XNNLO + combined HERA c/b DIS data set

Fits with varied $\overline{\mathrm{m}}_{\mathrm{c}}(\overline{\mathrm{m}}_{\mathrm{c}})$

Fits with varied small-x scale

$Q_0 = 1\ GeV; g(x, Q = 2\ \mathrm{GeV})$

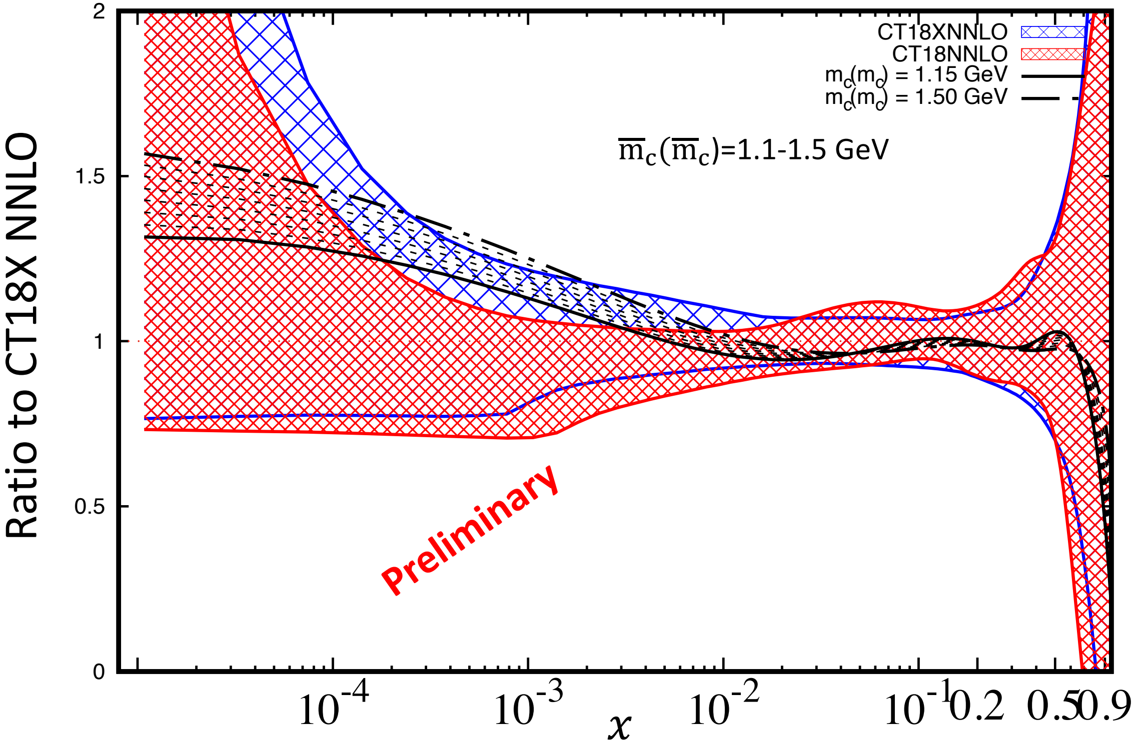

$Q_0 = 1\ GeV; g(x, Q = 2\ \mathrm{GeV})$

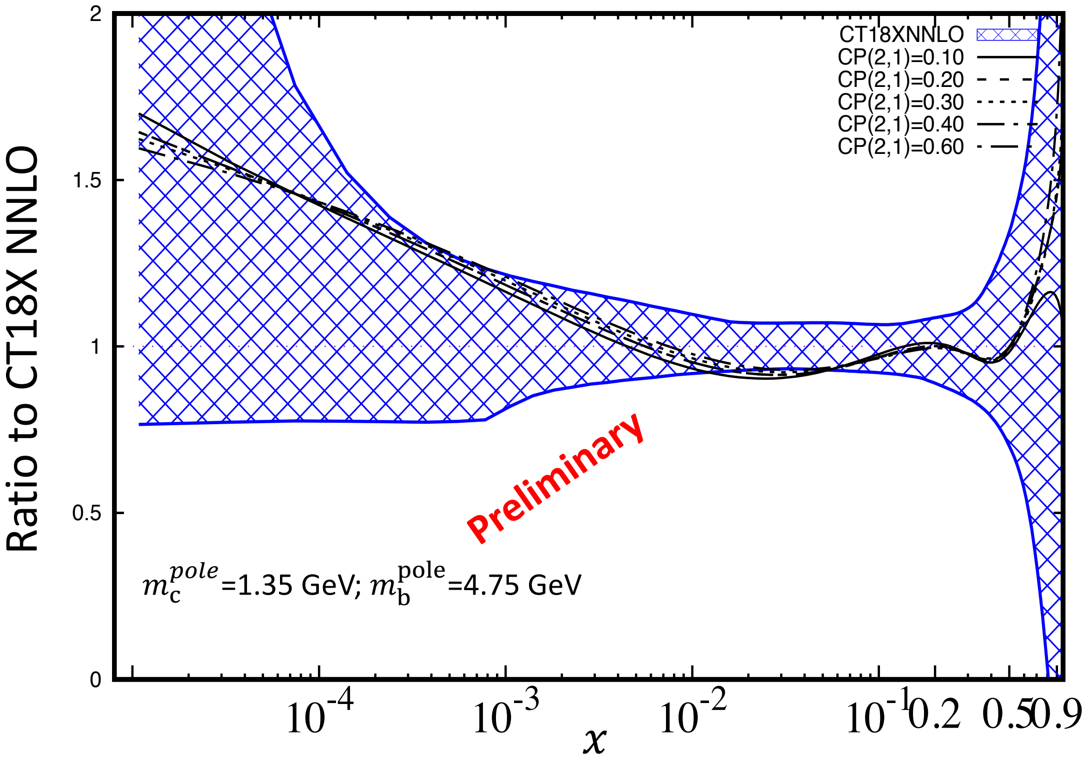

This data set mildly prefers CT18XNNLO to CT18NNLO.
But $\chi^2/\mathrm{N_{pt}}$ is never lower than 1.5 for all explored combinations

$$\mu_{DIS}(x) = A\sqrt{m_Q^2 + B^2/x^C}$$

Vary B=CP(2,1), while keeping A=0.5 and C=0.33 fixed

Conclusions

- These data are important because they also provide indirect constraints on strangeness.
- We tried to vary several parameters in the analysis. But in the best scenario, the $\chi 2$ /Npt is no lower than 1.5.
- All the fits we tried are tricky as parameters are correlated.
- We observe that these data seem to prefer a harder gluon in the intermediate/small x region.
- The $\chi 2$ /Npt which we find is similar to what has been found in MSHT20 and to the predictions from other groups reported in Tab 4 of 1804.01019 EPJC (2018) H1 and Zeus Coll.

The LUX formalism [1607.04266,1708.01256]

- The DIS process: $ep \to e + X$

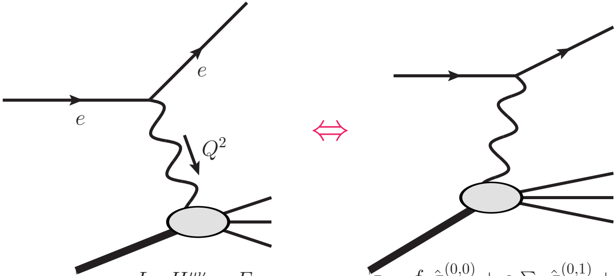

$\sigma \sim L_{\mu\nu} H^{\mu\nu} \sim F_{2,L}$ $\quad$ $\sigma \sim f_\gamma \hat{\sigma}^{(0,0)}_{\ell\gamma} + \alpha \sum_j \hat{\sigma}^{(0,1)}_{\ell j} + \cdots$

- Matching these two approaches leads to the LUX master formula:

$$x\gamma(x,\mu^2) = \frac{1}{2\pi\alpha(\mu^2)} \int_x^1 \frac{\mathrm{d}z}{z} \left\{ \int_{\frac{x^2 m_p^2}{1-z}}^{\frac{\mu^2}{1-z}} \frac{\mathrm{d}Q^2}{Q^2} \alpha_{\mathrm{ph}}^2(-Q^2) \left[\left(z p_{\gamma q}(z) + \frac{2x^2 m_q^2}{Q^2} \right) \times F_2(x/z, Q^2) - z^2 F_L(x/z, Q^2) \right] - \alpha^2(\mu^2) z^2 F_2(x/z, \mu^2) \right\}.$$

The square bracket term corresponds to the "physical factorization" scheme, while the second term is referred as the "$\overline{\mathrm{MS}}$-conversion" term.

- The structure functions $F_{2,L}$ can be directly measured, or calculated through pQCD in the high-energy regime.

The breakup of (x, Q^2) plane

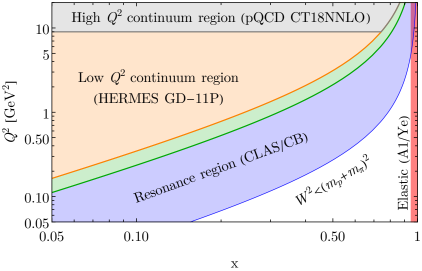

- In the resonance region $W^2 = m_p^2 + Q^2(1/x - 1) < W_{\rm lo}^2$, the structure functions are taken from CLAS [0301204] or Christy-Bosted [0712.3731] fits.
- In the low-Q^2 continuum region $W^2 > W_{\rm hi}^2$ GeV^2, the HERMES GD11-P [1103.5704] fits with ALLM [PLB1991] functional form.
- In the high-Q^2 region ($Q^2 > Q^2_{\rm PDF}$), $F_{2,L}$ are determined through pQCD.
- The elastic form factors are taken from A1 [1307.6227] or Ye [1707.09063] fits of world data.

The difference between LUX and DGLAP

- The DGLAP only evolves the inelastic photon

$$\frac{\mathrm{d}x\gamma^{\mathrm{inel}}}{\mathrm{d}\log\mu^2} = \frac{\alpha}{2\pi}\left(xP_{\gamma\gamma}\otimes x\gamma^{\mathrm{inel}} + \sum_i e_i^2 xP_{\gamma q}\otimes xq_i\right)$$

- The first-order solution corresponds to the LO F_2 in LUX formalism

$$x\gamma^{\mathrm{inel}}(x,\mu^2) \sim \int^{\mu^2} \mathrm{d}\log Q^2 \frac{\alpha}{2\pi}\sum_i e_i^2 xP_{\gamma q}\otimes xf_{q_i} \rightarrow F_2^{\mathrm{LO}} \text{ in LUX formula}$$

- It explains CT18qed gives larger photon at small x than CT18lux.
- MMHT2015qed gives smaller photon at small x, because the smaller charge-weighted singlet quark distributions.

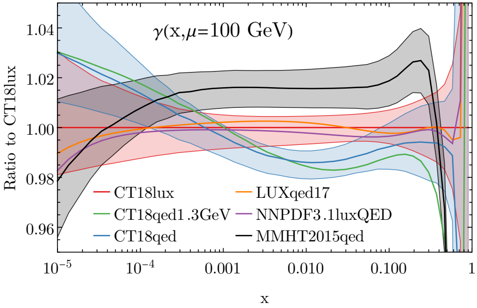

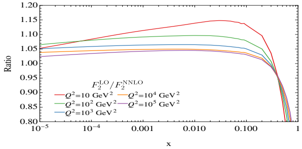

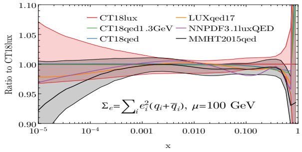

The large x behavior

- At large x, the LUX approach gives significantly larger PDF than the DGLAP one.
- It is resulted from the non-perturbative F_2 at low energy (resonance and low-Q^2 continuum regions).
- It induces a big uncertainty with the DGLAP low initialization scale approach, just because of scaling violation is not well behaved in the non-perturbative F_2.
- It can be rescued with a slightly higher initialization scale above the pQCD matching scale $Q_{\rm PDF} \sim 3$ GeV.

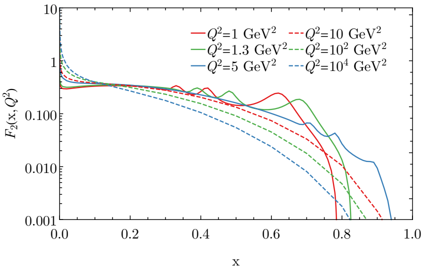

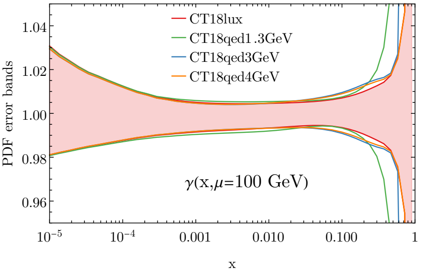

The cancellation in a higher order calculation

- Suppose we want to calculate a process $\gamma + X \to Y$.

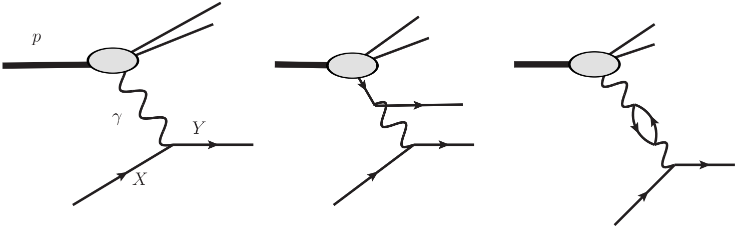

- At one order higher, both photon and quark parton will participate.
- The PDFs are related with the DGLAP evolution, with divergence properly canceled.
- This can be also achieved in the LUX approach, with proper $\overline{\mathrm{MS}}$ conversion terms order by order.

The scale variation of the $\overline{\mathrm{MS}}$ conversion term

- In the default scale choice $\mu^2/(1-z)$, the $\overline{\mathrm{MS}}$-conversion term is
$$x\gamma^{\mathrm{con}} \sim (-z^2)F_2(x/z,\mu^2),$$
which is negative
- When varying the scale as μ^2, the conversion term should be change as well,
$$x\gamma^{\mathrm{con}}([M]) = x\gamma^{\mathrm{con}} + \frac{1}{2\pi\alpha}\int_x^1 \frac{\mathrm{d}z}{z}\int_{M^2[z]}^{\frac{\mu^2}{1-z}} \frac{\mathrm{d}Q^2}{Q^2}\alpha^2 z p_{\gamma q}(z) F_2(x/z,Q^2).$$
With $M^2[z]=\mu^2$, we have $\int_{\mu^2}^{\frac{\mu^2}{1-z}} \frac{\mathrm{d}Q^2}{Q^2} = \log\frac{1}{1-z}$.
- The central MMHT2015qed corresponds to $M^2[z]=\mu^2$ choice at low scale $\mu_0 = 1\ \ \mathrm{GeV}$.
- The DGLAP approach at low scale DOES give larger uncertainty due to the large non-perturbative contributions to structure functions.
- One method to avoid it is to start γ PDF at a higher scale in the pQCD region, i.e., $\mu_0^2 > Q^2_{\mathrm{PDF}}$.

The DGLAP approach gives smaller PDFs at large x

- MMHT2015qed divides the integration into two regions:

$$\left(\int_{\frac{x^2 m_p^2}{1-z}}^{Q_0^2} + \int_{Q_0^2}^{\frac{Q_0^2}{1-z}}\right)[\cdots]$$

The second part is integrated semi-analytically:

$$\int_{Q_0^2}^{\frac{Q_0^2}{1-z}} \frac{\mathrm{d}Q^2}{Q^2}\alpha^2\left(zp_{\gamma q} + \frac{2x^2 m_p^2}{Q^2}\right)F_2(x/z, Q_0^2) = \alpha^2(Q_0^2)\left(zp_{\gamma q}\log\frac{1}{1-z} + \frac{2x^2 m_p^2 z}{Q_0^2}\right)F_2\left(\frac{x}{z}, Q_0^2\right)$$

The F_L is dropped because $F_L \sim \mathscr{O}(\alpha_s) \ll F_2$.

- In contrast, we integrate over $F_2(x/z, Q^2)$ rather than $F_2(x/z, Q_0^2)$.
- It explains the MMHT2015qed gives smaller photon at large x than CT18qed.
- MMHT15 does not include the uncertainty induced by Q_0 variation.

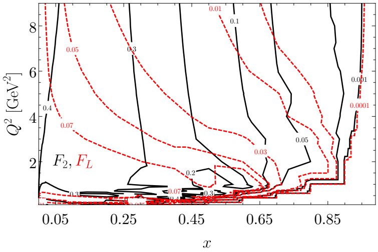

The NLO QED evolution and momentum sum rules

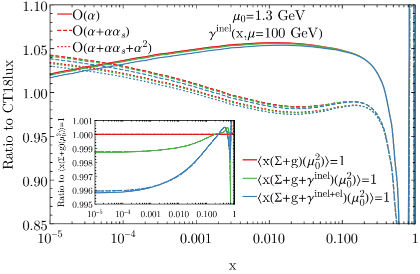

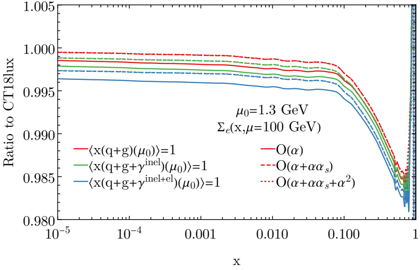

- The NLO QED corrections to splitting functions

$$P_{ij} = \frac{\alpha}{2\pi} P_{ij}^{(0,1)} + \frac{\alpha}{2\pi}\frac{\alpha_S}{2\pi} P_{i,j}^{(1,1)} + \left(\frac{\alpha}{2\pi}\right)^2 P_{ij}^{(0,2)} + \cdots$$

- The NLO QED correction is negative.
- The momentum sum rules: the impact is $\mathscr{O}(0.1\%)$, negligible compared with higher order QED evolution.

$$\langle x(\Sigma + g + \gamma^{\rm inel+el}\rangle = 1$$